Spectral Distribution of Cloud Cover over Africa

By I. Orlanski and L. J. Polinsky

Geophysical Fluid Dynamics Laboratories/NOAA Princeton University
(Manuscript received 17 May 1977, in revised form 16 July 1977)

Abstract

An analysis is made of the spectral characteristics of the cloud cover observed over Africa for a period of three months. The results indicate the predominance of a 2-2.7 day spectral peak within the vicinity of the Equator (10°N–10°S) with the intensity of this peak much stronger over land than over the ocean. The peak itself may not be detected if the smallest resolved area used in the data analysis is too large. Coherence was found to be maximum in belt-like configurations along certain latitude bands. The phase difference, although very noisy, indicates a horizontal scale on the order of 2000 kilometers.

1. Introduction

The recent GATE project in the tropical Atlantic provided a unique data set with which to investigate the dynamics of the equatorial atmosphere. It appears from the observational results which have been published so far that our previous understanding of the relationship between cloud clusters and the large-scale easterly waves which exist in those latitudes are not completely understood.

The idea that mesoscale systems in equatorial regions are primarily triggered by long waves has evolved from the erroneous belief that there are no other sources of large-scale motion in the tropical atmosphere that could organize extensive areas of convergence suitable for cloud clusters. The easterly waves since first observed by Riehl (1945) and Palmer (1951) were extensively discussed in the scientific literature by synoptic studies (Riehl, 1965; Yanai, 1961, 1963, 1968; Murakami, 1972; Reed and Recker, 1971), and by spectral analyses (Yanai *et al.*, 1968; Wallace and Chang, 1969; Nitta, 1970; Chang *et al.*, 1970; and Wallace, 1971). There is some evidence from those studies that easterly waves are generated by shear instability of the mean easterly flow (Lipps, 1970). The estimated wavelength of such waves is about 4000 km with periods of roughly 5 days. A more definitive result was obtained by the wind analysis of Burpee (1972) in which the 4 or 5 day peak was unquestionably present. The surprising observational result which emerged from GATE was that a considerable amount of variance in the cloud data and winds exists for periods less than 5 days and, more specifically, in the neighborhood of 2 days. Because of this fact, it appears that some other explanation is needed to describe the triggering of mesoscale systems in the equatorial belt.

A few years ago, Orlanski (1973) pointed out that a large amount of available potential energy, sufficient to generate large-scale internal waves, is contained in the oscillatory atmospheric boundary layer. The persistent oscillatory diurnal behavior of the atmospheric boundary layer is able to parametrically excite internal gravity waves. These waves are typically characterized by periods that could be twice as long as the diurnal forcing period. As discussed in Orlanski's paper, the maximum unstable waves depend on the latitude at which they are excited. In the equatorial belt, the maximum unstable waves will have periods close to 2 days and the horizontal scale is then fixed by the dispersion relation for waves with a vertical scale equal to the height of the diurnally varying boundary layer. In a numerical study, Orlanski (1976) showed that, for the equatorial atmosphere, the horizontal scales can be as large as 2000 kilometers. The horizontal direction of these waves is normally random; however, if the waves grow in the presence of a zonal flow, they will be oriented in rolls which are parallel to the mean wind.

Orlanski's (1976) comparison of the numerical simulation and the GATE results was very encouraging. However, Orlanski's proposed mechanism strongly depends on the diurnal variability

of the atmospheric stability. Although this variability is not very large over the ocean, the presence of these 2-day waves in ocean areas opens the possibility that these 2-day waves are either not related to the trapeze instability proposed by Orlanski, or if the trapeze mechanism is responsible for the 2-day waves, then the generating mechanism for such waves is very efficient. Consequently, an analysis of meteorological parameters over land, where the diurnal

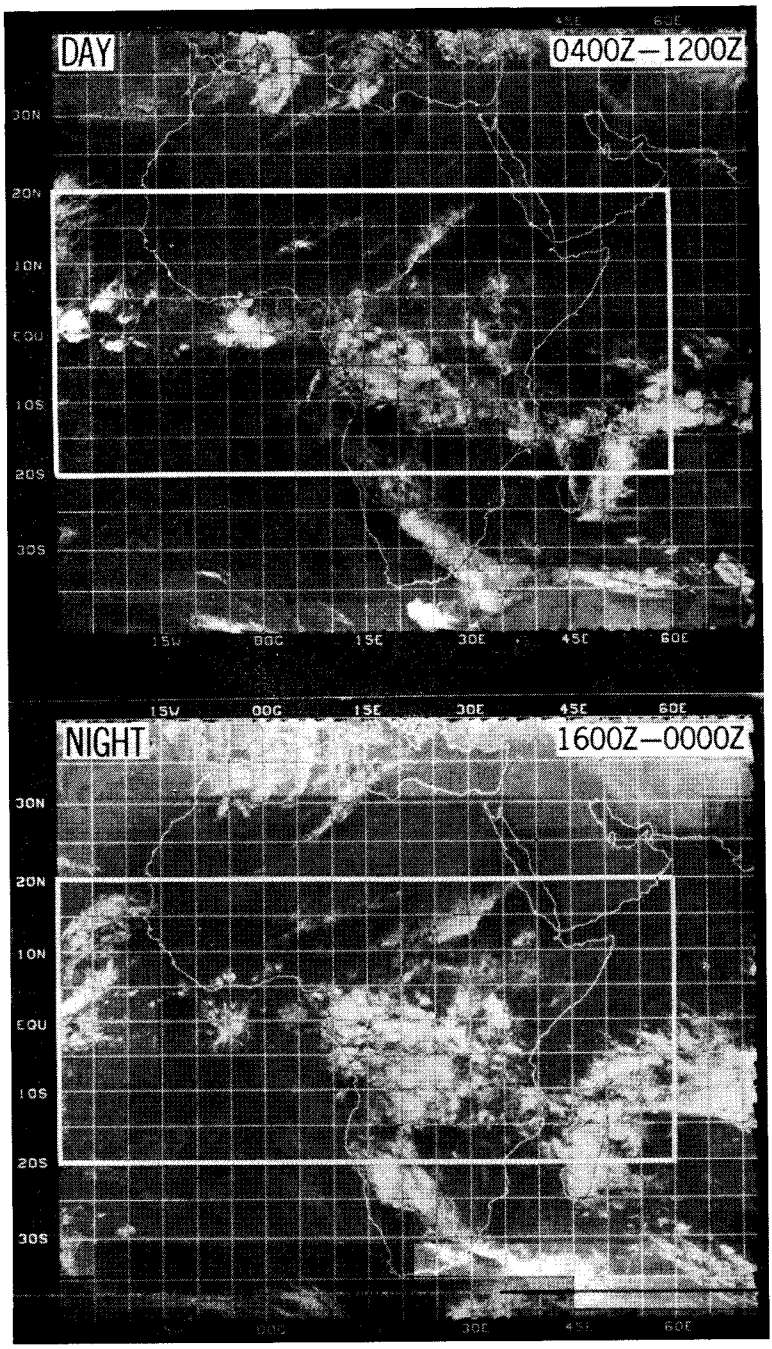

Fig. 1 A typical set of infrared day and night mosaics used in the analysis. The observational area is defined by the heavy white rectangle.

variability is large, must show a 2-day peak for the trapeze instability to be related to those waves.

It is therefore the purpose of this paper to discuss the spectral distribution of cloud cover over the African continent with particular emphasis on wave periods smaller than 4 days. Section 2 deals with the data acquisition and analysis, while in section 3 we shall discuss the results in terms of power spectra, variance, and coherence as a function of latitude and longitude. Finally, in section 4 we shall discuss the conclusions which we have derived from these results.

2. Data Aquisition and Analysis

The cloud data used in this study was obtained from the video output of the NOAA-4 polar-orbiting satellite. Mosaics from the infrared day and the infrared night observations were analyzed to obtain two daily cloud cover observations over the African domain. The satellite observations were taken over 3 hour intervals and centered about 0800Z (day obs.) and 2000Z (night obs.). An example of the mosaics used for this study is shown in Fig. 1. Cloud cover data used here is limited to an area bounded by 15°N to 20°S and 25°W to 60°E; approximately 45% of this region covers central and southern Africa. The area was then divided into 5° squares in which the cloud cover of the brightest upper 70% of the gray scale was considered and the area of cloud cover was estimated to the nearest one-tenth. The time records of cloud cover over the domain were fairly continuous. Missing data occurred in less than 5% of the total number of observations. The missing data was estimated by a linear interpolation in the time record. The temporal extension of the records was three months, beginning March 1, 1975 and ending May 31, 1975 thus providing 184 observations in each observational area. Using the digitized data, the computer recreated the satellite pictures by using a shade-plotting routine, and the shading was directly proportional to the cloud cover observed. The computerized pictures were then compared to the actual mosaics to correct any obvious error or bias in the interpolation of the missing data points.

The 144 records corresponding to each 5°× 5° box were analyzed by standard techniques such as the time lag power spectra and band-average FFT spectra. Since these methods are widely used in the literature, we will not mention the details related to them but rather refer the reader to Yanai, *et al.* (1968) or Hartmann (1974) for the particulars. Different time lags were used in the analysis; specifically, the results that we will show in the following sections have 10- and 15-day maximum time lags with the statistical assurance that the level of confidence is reasonably high when the maximum time lag is no more than 15% of the total record. An example of the power spectra of cloud cover is shown in Fig. 2 where the curves in the upper half of the figure correspond to a location of (5°N, 0°) and those in the lower half of the figure correspond to (10°S, 25°E). The three curves for each location represent the power spectra for 10 and 15 day maximum time lag for an area of 5°×5°

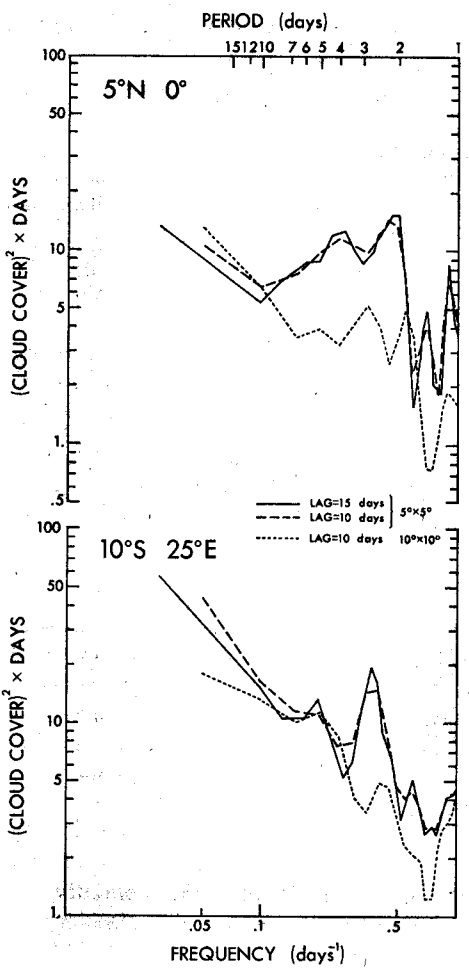

Fig. 2 Power spectra at 5°N, 0° and 10°S 25°E for 10 and 15 day lags in a 5°× 5° grid and a 10 day lag for a 10°× 10° grid.

and the power spectra for a maximum time lag of 10 days and an area of 10°×10°. Notice that the difference between the 10 and 15 day time lag for the same area is insignificant for the 5°×5° area analyses. Large differences can be seen however when the observational area is quadrupled as in the 10°×10° case. We will discuss these differences in more detail in another section. Moreover, the striking features that we can see in both locations, 5°N and 10°S, is the predominance of a peak in the neighborhood of 2 days and a secondary maximum around 4 or 5 days. In the following sections we will present more details of the power spectra, coherence, and phase differences as a function of latitude and longitude.

3. Results

a. Variance

The integration of the power spectra over 4 band frequencies was performed in order to obtain the variance. These bands were defined as follows: band 1 from 20 days to 10 days, band 2 from 10 days to 3.3 days, band 3 from 3.3 days to 1.67 days, and band 4 from 1.67 days to 1 day. Contours of the variance in units of (cloud cover)$^2\times10^2$ as a function of latitude and longitude are shown for the different bands in Figs. 3-6. One can immediately notice that bands 3 and 4 (Figs. 5 and 6), have the larger variance. In the latter two figures the contours of the variance extend in a belt-like fashion which resembles the position of the ITCZ at this time of the year as one would expect due to the high concentration of cloud cover. For comparative illustration, Fig. 7 shows monthly total precipitation areas over Africa for March 1975. Also, notice that the variance has strong maxima in two well-defined locations for bands, 2, 3 and 4. One maximum is located from the Equator to 10°S and from 20°E to 30°E; the other is centered in the western part of Africa along the Guinea Coast, specifically at (5°N, 0°). Power

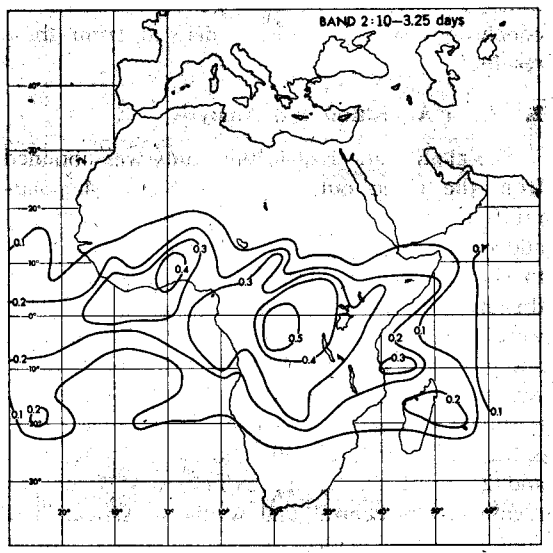

Fig. 4 As in Fig. 3 but for band 2 (10 days-3.25 days).

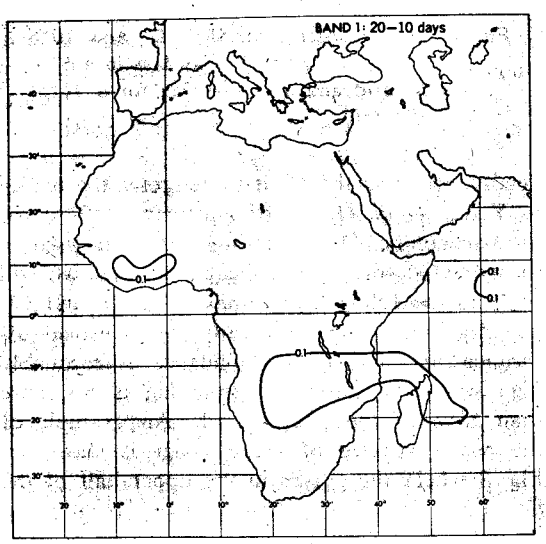

Fig. 3 Contours of variance for band 1 (3 months-10 days) in units of (cloud cover)$^2\times10^2$.

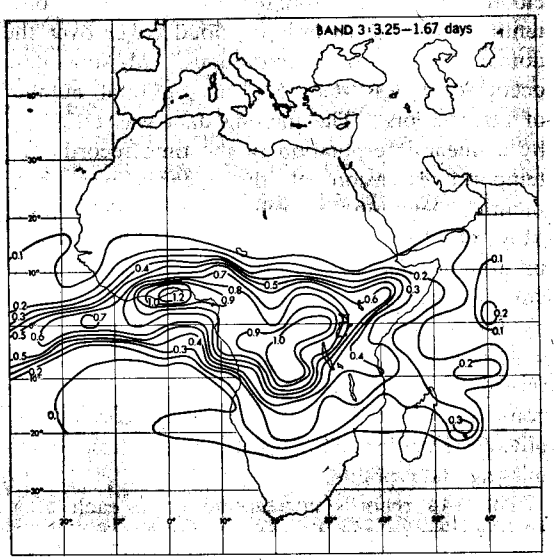

Fig. 5 As in Fig. 3 but for band 3 (3.25 days-1.7 days).

spectra along these maxima show interesting results as we shall see from the power spectra.

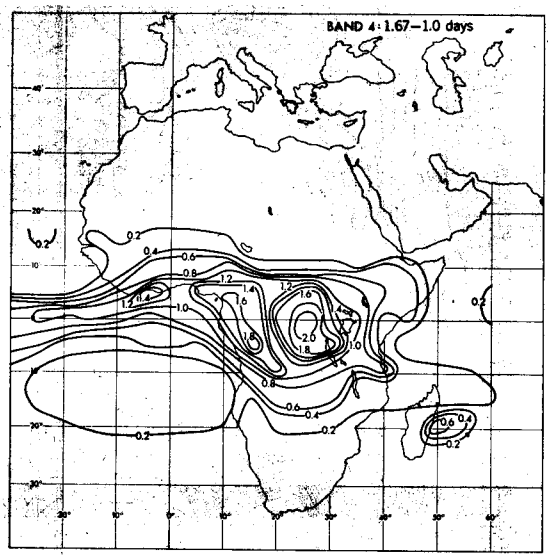

Fig. 6 As in Fig. 3 but for band 4 (1.7 days-1 day).

b. Power Spectra

Initially, we will consider the former of the maxima discussed in the previous sub-section, *i.e.* the equatorial maximum in the center of the continent. The power spectra shown in Fig. 8 was calculated with a 10 day maximum lag along 25°E longitude. Notice the intense maximum around 5 days over the Equator and a secondary maximum at about 2.5 days extending from the Equator to 10°S. The diurnal maximum is close to the Nyquist frequency due to our two daily observations; therefore, we shall not discuss it here nor shall we discuss the large power spectra for periods longer than 10 days because of the temporal limits of our records. In order to verify that the time lag power spectra is consistent with the results of other analysis methods, we have also calculated the band average fast Fourier spectra using the full record. The results of this calculation along the same longitude are shown in Fig. 9. The similarities between the location and intensity of the spectral peaks are clearly seen. In view of this comparison, the time lag power spectra appears to be somewhat smoother

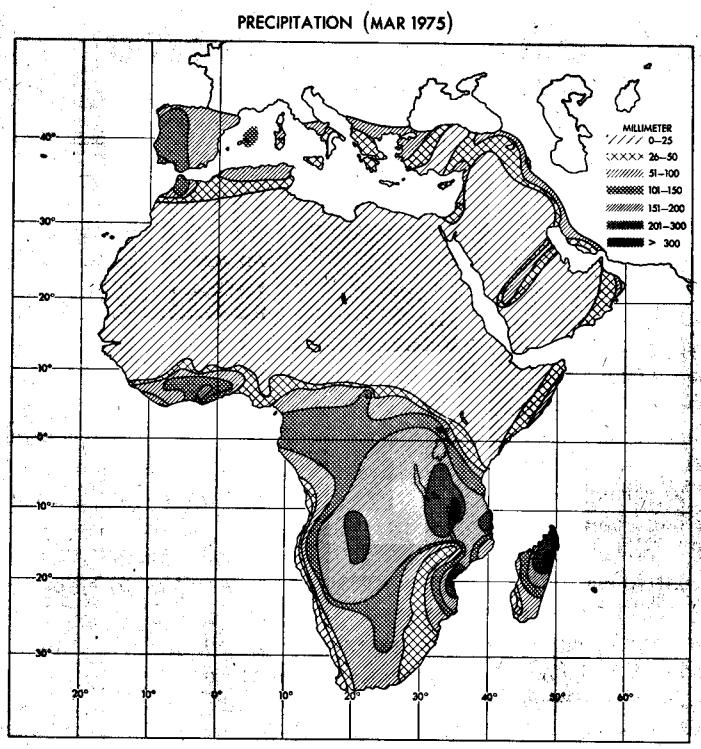

Fig. 7 Total precipitation for March 1975 over Africa and surrounding islands and also including parts of southern Europe and the Near East. (Monthly Climatic Data for the World, March 1975).

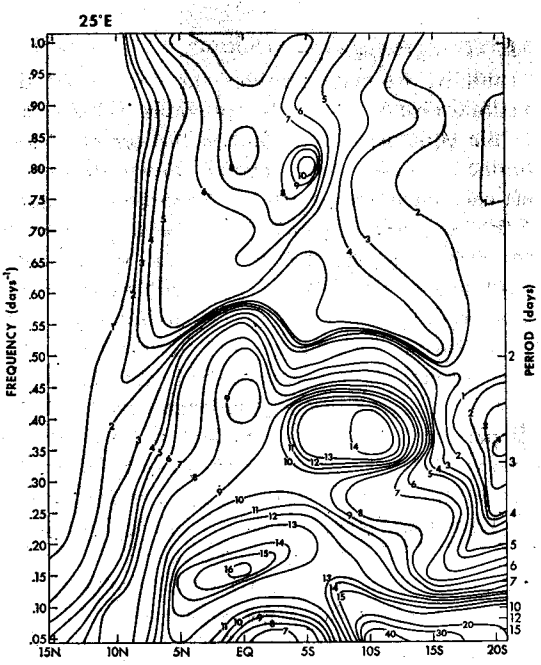

Fig. 8 The 10 day lag power spectra at 25°E as a function of latitude.

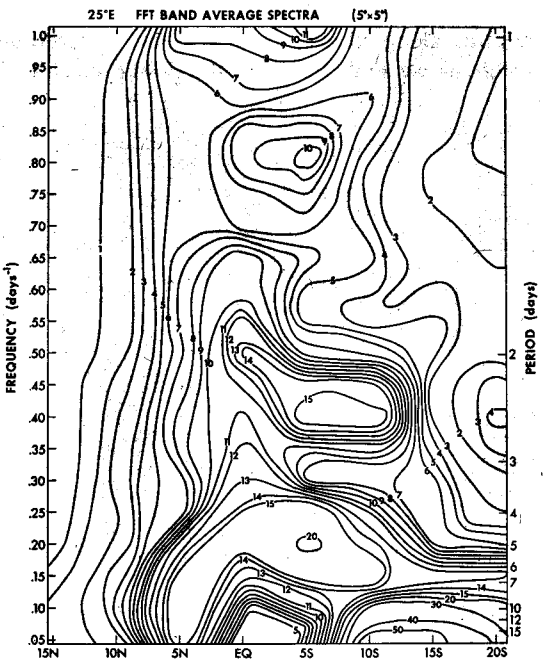

Fig. 9 The FFT power spectra at 25°E as a function of latitude.

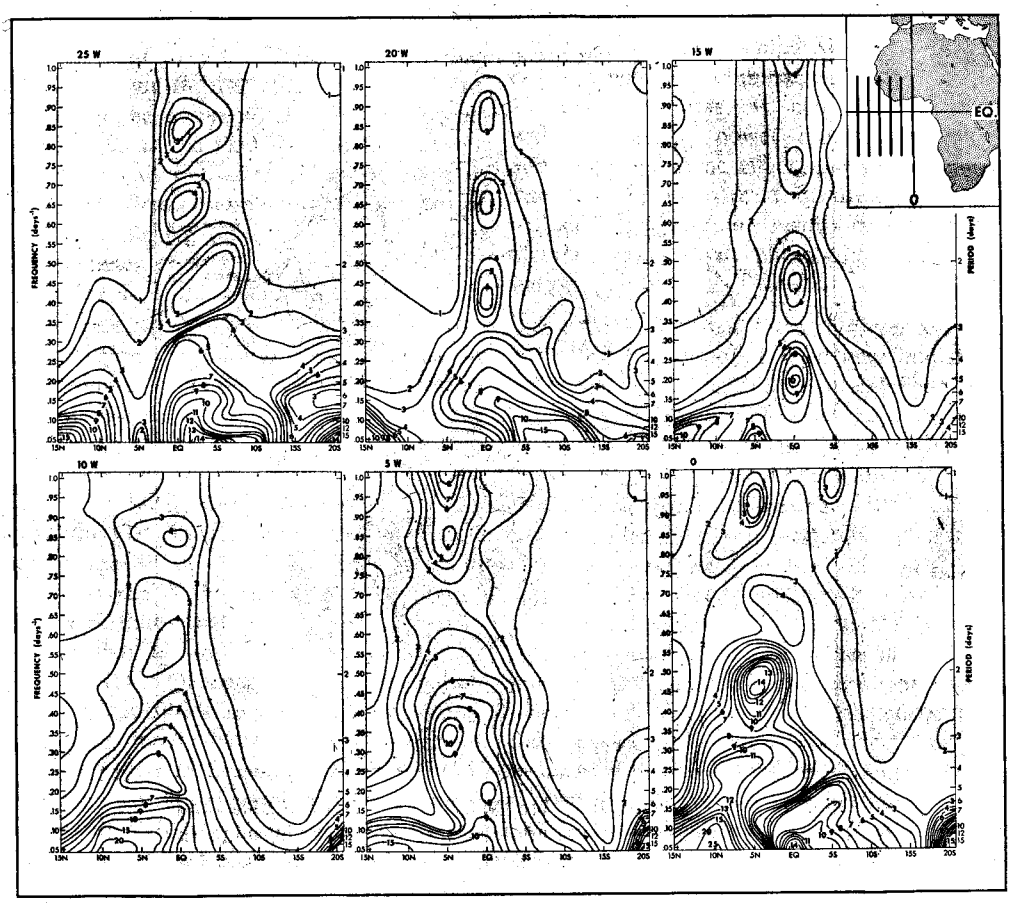

Fig. 10 The 10 day lag power spectra as a function of latitude from 25°W to 0° longitude.

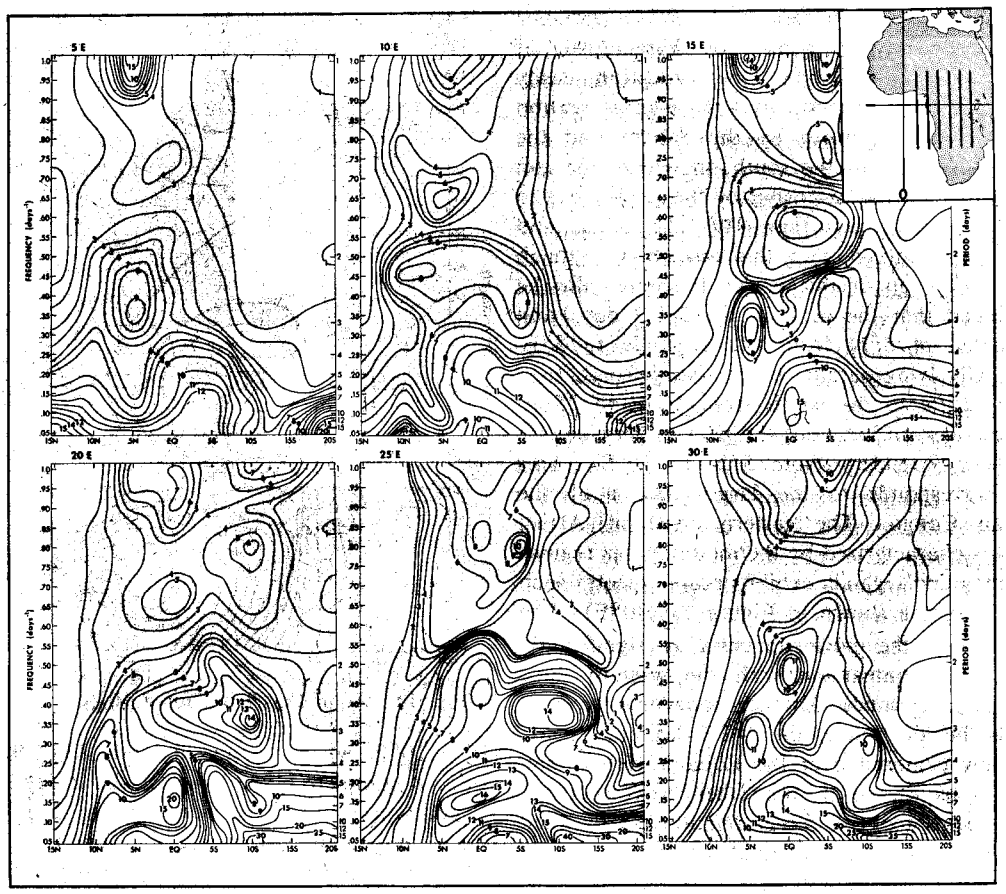

Fig. 11 As in Fig. 10 but from 5°E to 30°E.

than the FFT band average spectra.

The two predominant peaks observed in Figure 8, that is, the 4–5 and 2–2.7 day peaks, can be detected not only at one particular longitude, such as 25°E as shown in Figure 8, but rather seems to be a feature of the spectra at all longitudes in the observation area. Figures 10 and 11 show the power spectra as a function of latitude for the longitudes analyzed. The locations of the cross sections are shown on the insert map of Africa which appears in the upper right corner of each figure. A feature that one can readily notice is that some of the cross sections are only over the ocean, some are partially over land and ocean, and others are entirely over land. This allows us the opportunity to in some way detect the influence of the lower boundary on the predominant maximum peaks in the spectra. The graphs in Figure 10 from 25°W-15°W have a very low level of variance throughout the region; however, one may still identify a peak in the neighborhood of 2 days that increases in intensity moving from west to east. The diurnal variability nevertheless seems to be very weak or nonexistent. Variance in the 4 to 5 day range is noticeable, but not as a distinct peak. Moving further eastward, the lower graphs of Figure 10, we observe considerable intensification of the diurnal variability as well as the variance of the 2–2.7 day band. A similar increase in variance is also observed for longer periods. It is interesting to compare the spectra of the figure to those of 5°W and 0° longitude and note that the latter spectra shift 5° northward. This is simply explained by the position of the African land mass as can be seen in the insert. In fact, we might also add that the location of those peaks follows the position of the ITCZ. These results are perhaps not independent of the fact that we are analyzing cloud cover and it would seem obvious that one would expect the maximum variance to coincide with the position of the ITCZ. The intensity of the power spectra increases more dramatically for the eastern cross sections as seen

in Figure 11. A considerable amount of variance for periods close to 1 day are characteristic of the spectra over land. One exception easily noticed is in the spectra of 5°E, a cross section bounded on the north by the Sahara and the Gulf of Guinea to the south, in which one can notice the narrow extension of the peak close to 1 day which is less than 10°; the other land spectra in contrast with this one show a much wider extension of this peak. It should also be mentioned that the peak in the 2–2.7 day band is located at 5°N from 0° longitude to 5°E, practically lying parallel to the Ivory Coast, then slowly drifts to the south from 10°E to 25°E. In these eastern locations the peak is very intense and very extended (from 5°N to 10°S). This area corresponds to the large plateau of the African Congo. The eastern coast of Africa which is characterized by the mountainous regions of Kenya and Uganda exhibits power spectra such as the last one shown in Figure 11 (30°E). The variance of the power spectra is significantly reduced in comparison with the western most locations over land. Another noteworthy feature here is the location of the 2–2.7 day band peak; it is now centered over the Equator rather than at 10°S as shown in the other cross sections. There seems to be a direct relationship between the spectral peak at the Equator and the position of Lake Victoria as well as a lack of variance to the south of it corresponding to the highlands of Tanzania. Overall, we must conclude that there is a large variance present in the 2–2.7 day band and that there is a correlation between the intensity and extension of the peak and its geographical position. A similar analysis done by Gruber (personal communication) of satellite pictures of cloud cover over western Africa, the GATE area, and South America tends to show a similar behavior in the power spectra with respect to the 2–2.7 days peaks over western Africa and the GATE area, his results also show a reduced intensity of the 2–2.7 days peak in comparison to the 5 day peak. The only difference other than the geographical location seems to be that he took a minimum analysis area of 10°×10°. Of course, if the mesoscale systems which contribute to the 2–2.7 day bands in our spectra have scales on the order of 1000 km or smaller, that would explain this discrepancy. To test this possibility, we analyzed our data in 10°×10° squares. Results of this analysis are shown in Fig. 12 which shows the power spectra for the larger horizontal area

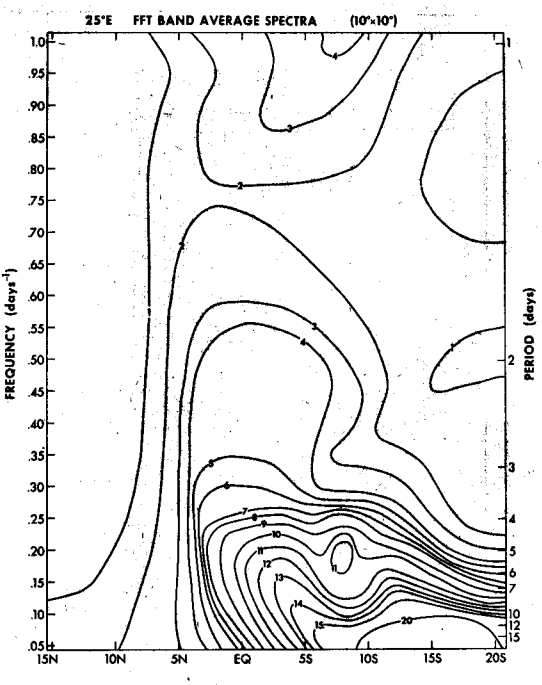

Fig. 12 As in Fig. 9 but for a 10°×10° grid.

(10°×10°); when compared with Fig. 9, we notice a complete elimination of the 2-day peak. In addition to this, we can refer to Fig. 2 in which individual power spectra for 10°S and 5°N show the same effect. To gain some insight into the scales involved in these processes, we will now examine the results of an analysis of the coherence and phase difference between stations.

c. Coherence and Phase Difference

The analysis program used here and described by Yanai, *et al.* (1968) can calculate the coherence and phase difference between two stations. The coherence and phase differences to be presented were calculated with respect to two reference centers, one between (10°S, 25°E) and all the other stations, and the other between (5°N, 0°) and all the other stations. Fig. 13 shows the contours of coherence as a function of latitude and longitude in which the light shaded areas designate coherence values larger than 0.5 and the dark shaded areas represent regions of coherence larger than 0.6. This particular case is for a period of 5 days. The heavy lines outline the change in sign of the phase angle. However, we feel that the phase lines outside the areas of large coherence are not very reliable. Nevertheless, the east-west separation of the phase lines near the equator indicates the scale of the dis-

turbance to be on the order of 6000 km. Similar analyses were done for the 2-day disturbance at the locations (10°S, 25°E) and (5°N, 0°) as can be seen in Figs. 14–15. Although the coherence was reasonably high, the phase angle was found to change abruptly from station to station. Phase lines in figures 14 and 15 suggest a rough estimation of 2000 km for the east-west scale. This result is only suggestive since our resolution was 5° and only 3 or 4 points will correspond to a wavelength. Moreover, the calculated phase difference and its orientation has no relevance in this particular case since these waves could come in bursts of 10 or 15 days, and looking at the phase differences obtained over 3 months time is not appropriate. However, some rough estimation of the scale, as well as the orientation, is possible. Unfortunately, we do not have information on the mean wind systems for this time period although the derived phase orientation of the waves seems to imply the existence of a north-south wind. This result is also consistent with the previous discussion of the differences in power spectra between analyses areas of 5°×5° and 10°×10° as shown in Figs. 9 and 13.

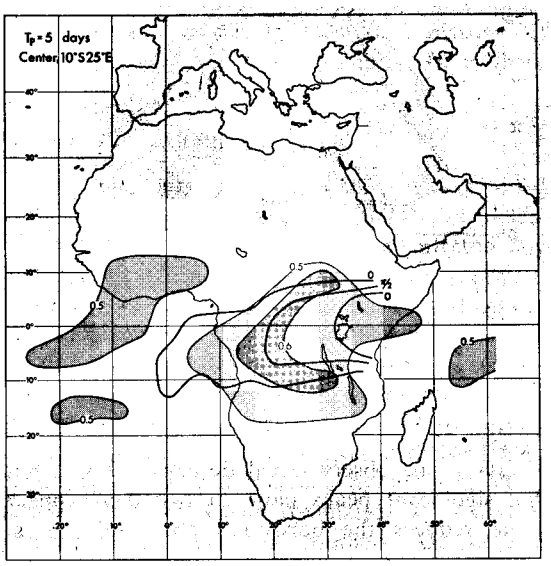

Fig. 13 Contours of coherence greater than 0.5 for T_p=5 days. Heavy lines denote the changes in phase angle.

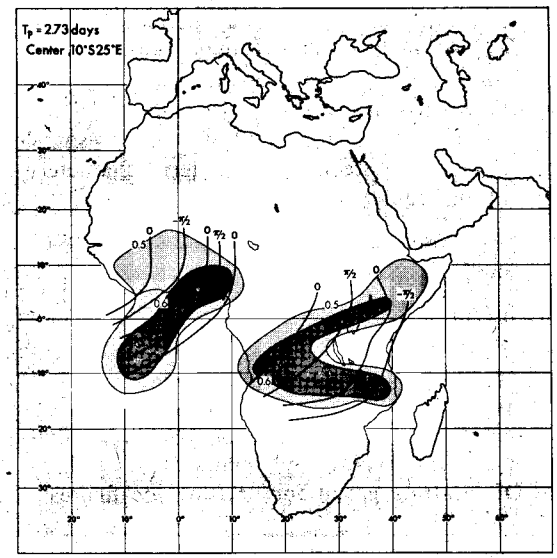

Fig. 14 As in Fig. 13 but for T_p=2.73 days.

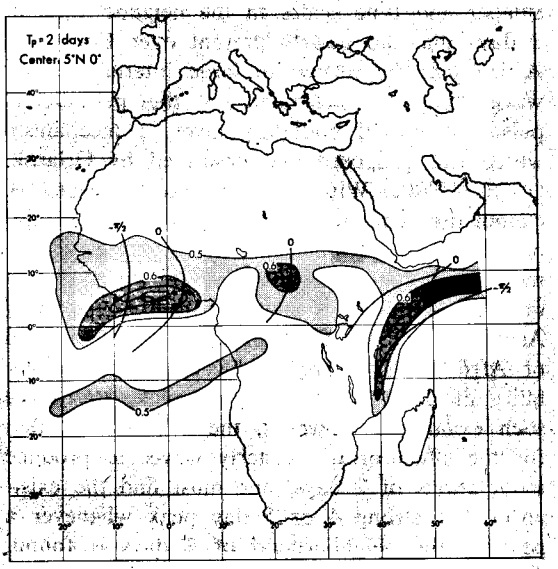

Fig. 15 As in Fig. 14 but for T_p=2 days.

4. Discussion and Conclusions

From the observational analyses presented here, one may conclude that a large amount of the cloud cover variance exists in periods close to 2 days (40%), that there are two centers where the 2–2.7 days peak is a maximum (10°S, 25°E and 5°N, 0°), and that the power spectra maxima at the 2–2.7 day band depends on the smallest resolved area used in the data analysis.

The power spectra peak 2–2.7 days waves is considerably larger over land than over the ocean. Coherence was found to be maximum in belt-like configurations along certain latitude bands. The phase difference, although very noisy, indicates a horizontal scale on the order of 2000 km.

It seems appropriate to suggest that mesoscale systems with scales of the order of 1000 km or

smaller and time scales in the neighborhood of 2 days that are clearly present over Equatorial Africa may be related to large internal gravity waves that are generated by the periodically pulsating diurnal boundary layer, a mechanism which was proposed and described by Orlanski (1973, 1976). With this analysis however, we cannot discount other processes which could also contribute to periodicities discussed here. The modulation effect produced by the easterly waves in the precipitation patterns as discussed by Asplinden, *et al.* (1976) and, that the generation of African waves are produced by shear instability of the low level jet (Rennick, 1976) are such examples. However, the authors feel that for the effect of the easterly waves to produce modulations of 2 days, one must find the existence of a strong 4 or 5 day peak whenever a peak in the neighborhood of 2 days is found. As Figure 11 shows, this is not the case. As to the possibility of some kind of shear instability of a mean flow as proposed by Rennick, we cannot claim or disclaim much from this data. Perhaps with wind spectra we could learn more about this possibility; however, we feel that the local topographic control that seems to appear in this data is in contradiction to what one would expect if the processes were generated by some kind of instability of the easterly zonal flow. Clearly, from Figures 10 and 11 one can dispute the possibility that the maximum instability for those waves is located at 14°N as claimed by Rennick. Rather, it seems that the maximum activity is controlled by the characteristics of the lower boundary layer and strongly dependent on longitude which is contrary to Rennick's conclusions.

Realizing that the data is not as complete as one would like to have, we sincerely feel that this analysis in some way disproves some of the generating mechanisms previously proposed and although not conclusive, it tends to be consistent with the suggested possibility that trapeze instability is a possible mechanism by which mesoscale systems in Equatorial regions are formed. Clearly, more analyses will be needed to elucidate the sources of these highly active mesoscale processes. Figure 16 shows the contribution of each band average of variance in relation to the average cloud cover. We must conclude from this figure that the average variance is primarily contained in periods less than 3 days. Murakami (1972) showed that, over the Marshall Islands, the maximum peak of the vertical velocity is at

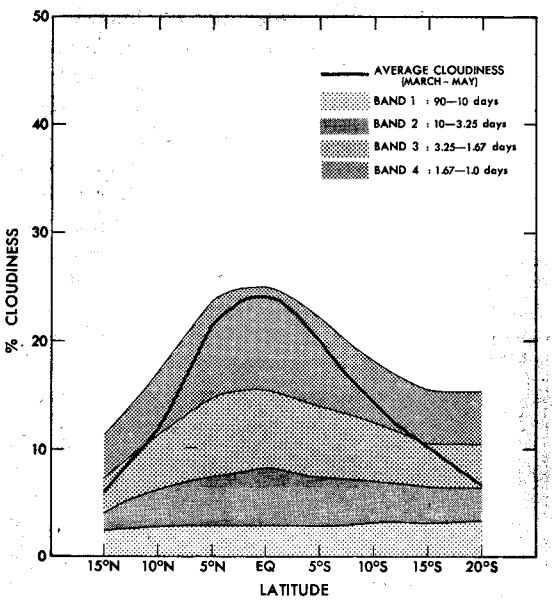

Fig. 16 A comparison between the average cloudiness for the 3 month period (Mar-May 1975) and the square root of each band average contribution of variance.

5 days if the observational domain is large, but that significant peaks close to two days appear if he reduces the horizontal observation area. This result is very much in agreement with our comparative analysis of 5°×5° and 10°×10° spectra.

Although the results of this study are highly suggestive of the existence of a mesoscale phenomena with close to two day periodicity, more analysis of high resolution data, both in space and time for different meteorological variables, will be needed in order to more fully understand the dynamics and the role of such mesoscale processes in the precipitation patterns characteristics of the equatorial regions.

Acknowledgements

We would like to thank Dr. Y. Hayashi for his useful suggestions and to Drs. G. Philander and B. Ross for reading the manuscript and providing their comments which helped to clarify the paper. We would also like to thank Helen Franckowiak for keypunching the data, Betty Williams for typing the manuscript, and the GFDL drafting group for drafting the figures.

References

Asplinden, C. I., Y. Tourre and J. B. Sabine, 1976:

Some climatological, aspects of West African disturbance lines during GATE. *Mon. Wea. Rev.*, **104**, 1029–1035.

Burpee, R. W., 1972: The origin and structure of easterly waves in the lower troposphere of North Africa. *J. Atmos. Sci.*, **29**, 77–90.

Chang, C. P., V. F. Morris and J. M. Wallace, 1970: A statistical study of easterly waves in the Western Pacific: July-December 1964. *J. Atmos. Sci.*, **27**, 195–201.

Hartmann, D. L., 1974: A time spectral analysis of mid-latitude disturbances. *Mon. Wea. Rev.*, **102**, 348–362.

Lipps, F. B., 1970: Barotropic stability and tropical disturbances. *Mon. Wea. Rev.*, **98**, 122–131.

"Monthly Climatic Data for the World," March 1975, **28**, 3, U.S. Dept. of Comm., NOAA, E.D.S.

Murakami, M., 1972: Intermediate scale disturbances appearing in the ITC Zone in the tropical western Pacific. *J. Meteor. Soc.*, **50**, 454–464.

Nitta, T., 1970: Statistical study of tropospheric wave disturbances in the tropical Pacific region. *J. Meteor. Soc.*, **48**, 47–60.

Orlanski, I., 1973: Trapeze instability as a source of internal gravity waves, Part I. *J. Atmos. Sci.*, **30**, 1007–1016.

————, 1976: The trapeze instability in an equatorial β-plane. *J. Atmos. Sci.*, **30**, 1007–1016.

Palmer, C. E., 1951: Tropical meteorology. Compendium of Meteorology. *Amer. Meteor. Soc.*,

Rennick, M. A., 1976: The generation of African waves. *J. Atmos. Sci.*, **33**, 1955, 1969.

Riehl, H., 1945: "Waves in the easterlies and the polar front in the tropics." Dept. Meteor., Univ. Chicago, Misc. Rept. No. 17, 79 pp.

————, 1965: Varying structure of waves in the easterlies. Proc. Intern. Symp. on Dynamics of Large-Scale Processes. Moscow, 411–416.

Wallace, J. M., 1971: Spectral studies of tropospheric wave disturbances in the tropical western Pacific. *Rev. Geophys.*, **9**, 557–612.

————, and C.-P. Chang, 1969: Spectrum analysis of large-scale wave disturbances in the tropical lower troposphere. *J. Atmos. Sci.*, **26**, 1010–1025.

Yanai, M., 1961: A detailed analysis of typhoon formation. *J. Meteor. Soc. Japan*, **39**, 187–214.

————, 1963: A preliminary survey of large scale disturbances over the tropical Pacific region. *Geofis. Intern.* (Mexico), **3**, 73–84.

————, 1968: Evolution of a tropical disturbance in the Caribbean Sea region. *J. Meteor. Soc.*, **46**, 85–109.

————, T. Maruyama, T. Nitta and Y. Hayashi, 1968: Power spectra of large-scale disturbances over the tropical Pacific. *J. Meteor. Soc.*, **46**, 308–323.

アリフカ上空の雲量のスペクトル解析

I. Orlanski and L. J. Polinsky

プリンストン大学

3カ月の期間についてアフリカ上空の雲量のスペクトル解析を行った。解析の結果は，赤道附近 (10°N～10°S) における2～2.7日周期帯における顕著なスペクトルピークを示している。このピークは，海上においてよりも，陸上においてより著しい。解析に使用する面積平均雲量を求めるさいの面積が大きすぎると，このピークは求められない。コヒーレンスの分布は，ある緯度帯にそう帯状の分布を示している。位相差の分布はかなり乱れているが，現象の水平スケールが約2,000 km であることを示している。

Atmospheric and Oceanic Heat Export in the Tropical Pacific

By Stefan Hastenrath

The University of Wisconsin
(Manuscript received 20 May 1977, in revised form 3 August 1977)

Abstract

A partitioning of heat export by the oceanic water body vs. the atmospheric column is presented for the tropical Pacific, on the basis of satellite-derived net radiation at the top of the atmosphere and calculations of the oceanic heat budget. For individual Marsden squares, the divergence of heat transport within the oceanic water body ranges from +169 (export) to −191 (import) percent of the net radiative input to the system at the top of the atmosphere. Heat export within the ocean is particularly important in the band of cold water immediately to the South of the Equator.

1. Introduction

The low latitudes are the input region to the global heat budget. The net radiative heat gain at the top of the atmosphere is exported poleward within both atmosphere and ocean. Satellite measurements of net radiation at the upper boundary of the earth-atmosphere system and computations of the oceanic heat budget invite a reappraisal of the relative importance of tropical atmosphere and ocean in global energetics. This has recently been performed for the tropical Atlantic Ocean (Hastenrath, 1977). In complementation of that work, the present paper attempts an evaluation for the tropical Pacific.

The long-term average annual heat budget of the Pacific Ocean has been calculated by Wyrtki (1965). His charts permit an evaluation by five degree square areas. Satellite-derived net radiation data for the top of the atmosphere over a few years have been published recently (Vonder Haar and Ellis, 1974), but these refer to the middle of ten degree squares. These publications provide the data base for the present study. Ocean areas evaluated here are shown in Fig. 1.

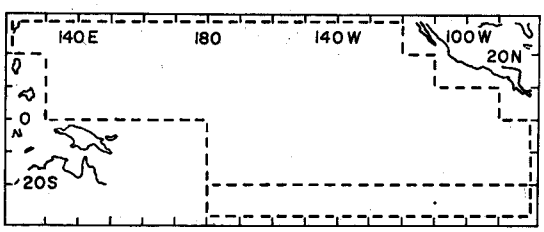

Fig. 1 Orientation map. Broken line blocks indicate data coverage for Fig. 3 and Table 1.

2. Basic theory

A heat budget scheme for the atmosphere—ocean system is presented in Fig. 2. The budget equation for the system as a whole can be written

$$\mathrm{SWLW}\uparrow\downarrow_{top}=Q_{va}+Q_{ta}+Q_{vo}+Q_{to} \qquad (1)$$

The left-hand term signifies the net radiation at the top of the atmosphere; in the right-hand terms the subscripts v and t denote divergence of heat transport and storage, respectively, the subscripts a and o referring to atmosphere and ocean.

The heat budget equation for the atmospheric column reads

$$Q_{va}+Q_{ta}=[\mathrm{SWLW}\uparrow\downarrow_{top}-\mathrm{SWLW}\uparrow\downarrow_{sfc}] +e+Q_s \qquad (2)$$

where the right hand terms denote the net radiative cooling of the atmospheric column, latent and sensible heat transfer at the ocean surface, respectively.

For the heat budget of the ocean

$$\mathrm{SWLW}\uparrow\downarrow_{sfc}=Q_e+Q_s+Q_{vo}+Q_{to} \qquad (3)$$

the left-hand term being the net radiation at the ocean surface. This in turn is equal to the sum of net shortwave, $\mathrm{SW}\uparrow\downarrow_{sfc}$, and net longwave radiation $\mathrm{LW}\uparrow\downarrow_{sfc}$, at the surface.

Addition of Eqs. (2) and (3) yields Eq. (1),